Research Square

Preprints are preliminary reports that have not undergone peer review.
They should not be considered conclusive, used to inform clinical practice,
or referenced by the media as validated information.

MET–ERK–HIF1A signaling regulates CAV2-mediated cancer stemness in non-small cell lung cancer

Shuxi Yao[1]
Tongji Hospital, Tongji Medical College, Huazhong University of Science and Technology
Jie Tong[1]
Tongji Hospital, Tongji Medical College, Huazhong University of Science and Technology
Yutao Zhang[1]
Tongji Hospital, Tongji Medical College, Huazhong University of Science and Technology
Yiming Li[1]
Tongji Hospital, Tongji Medical College, Huazhong University of Science and Technology
Yanqi Feng[1]
Tongji Hospital, Tongji Medical College, Huazhong University of Science and Technology
Kunrui Zhu[1]
Tongji Hospital, Tongji Medical College, Huazhong University of Science and Technology
Xinyue Liu[1]
Tongji Hospital, Tongji Medical College, Huazhong University of Science and Technology
Xiangtian Xiao[1]
Tongji Hospital, Tongji Medical College, Huazhong University of Science and Technology
Yuelin Han[1]
Tongji Hospital, Tongji Medical College, Huazhong University of Science and Technology
Zhuoyan Han[1]
Tongji Hospital, Tongji Medical College, Huazhong University of Science and Technology
Dawei Ye[1]
Tongji Hospital, Tongji Medical College, Huazhong University of Science and Technology
Shu Xia[1]
xiashutj@hust.edu.cn

Tongji Hospital, Tongji Medical College, Huazhong University of Science and Technology

Research Article

Keywords: NSCLC, MET amplification, CAV2, cancer stemness, HIF1A, ERK signaling, crizotinib

Posted Date: November 25th, 2026

DOI: https://doi.org/10.21203/rs.3.rs-11480302/v1

License: This work is licensed under a Creative Commons Attribution 4.0 International License.
Read Full License

Additional Declarations: No competing interests reported.

Abstract

Background

MET amplification is a clinically actionable oncogenic alteration in non-small cell lung cancer (NSCLC), but the mechanisms linking MET signaling to cancer stemness and treatment response remain incompletely understood. We investigated whether caveolin-2 (CAV2) mediates MET-associated stemness and affects the response to crizotinib.

Methods

We integrated TCGA and CCLE datasets to identify genes associated with MET expression. The relationship between MET status and CAV2 expression was examined by immunohistochemistry in a retrospective cohort of 40 NSCLC specimens. Survival associations were evaluated separately in an independent public NSCLC cohort. The function of CAV2 was investigated using gene knockdown, tumorsphere assays, flow cytometry, analysis of stemness-associated markers, and limiting dilution xenograft assays. Pathway inhibition, luciferase reporter assays, and chromatin immunoprecipitation were used to examine the underlying mechanism. The effect of CAV2 depletion on the response to crizotinib was assessed in vitro and in xenograft models.

Results

CAV2 was identified as a MET-associated gene and was highly expressed in MET-amplified NSCLC models. In the retrospective tissue cohort, CAV2 H-scores were higher in MET-FISH-positive tumors than in MET-FISH-negative tumors and correlated positively with MET H-scores. In an independent public NSCLC cohort, high CAV2 expression was associated with shorter overall and progression-free survival. CAV2 depletion reduced tumorsphere formation, CD44-positive stem-like populations, stemness-associated marker expression, and tumor-initiating capacity. In experimental models, MET-associated signaling increased CAV2 transcription through the ERK-HIF1A pathway, and HIF-1α occupied the CAV2 promoter. CAV2 depletion shifted the crizotinib dose-response curve in vitro, and combined CAV2 depletion and crizotinib treatment reduced xenograft tumor burden more than either intervention alone.

Conclusions

These findings support CAV2 as a downstream mediator of MET-associated stemness in experimental NSCLC models. CAV2 depletion also increased the antitumor effect of crizotinib, suggesting that CAV2-dependent stemness programs warrant further investigation as therapeutic targets in MET-amplified NSCLC.

1. Introduction

Cancer stem cells (CSCs) are tumor cell subpopulations with self-renewal and tumor-initiating capacities that contribute to cancer progression, metastasis, and treatment resistance [1–4]. Evidence from NSCLC supports the presence of stem-like tumor cells that participate in disease progression and metastatic dissemination [5]. However, the signaling networks that maintain these cellular states remain incompletely defined. Identifying these networks may reveal vulnerabilities that complement existing treatments for NSCLC.

The receptor tyrosine kinase MET is an established oncogenic driver in NSCLC. Aberrant MET activation, commonly caused by gene amplification or mutation, promotes tumor progression and is associated with adverse outcomes and treatment resistance [6–11]. Although MET-targeted therapies benefit selected patients, acquired resistance frequently limits the duration of response [12–16] MET signaling has also been linked to cancer stem-like properties in several malignancies [17, 18], but the mechanisms connecting oncogenic MET signaling to stemness in NSCLC are not fully understood.

Caveolae are cholesterol- and sphingolipid-rich plasma membrane invaginations that organize signal transduction [19–21]. Their principal structural proteins, caveolin-1 (CAV1) and caveolin-2 (CAV2), regulate receptor trafficking and pathways involved in cell proliferation, survival, and migration [22]. CAV2 has context-dependent functions in cancer, and increased CAV2 expression has been associated with aggressive behavior and poor outcomes in several tumor types, including NSCLC [23–25]. Recent evidence also implicates CAV2 in cancer stem-like phenotypes [26]. Whether CAV2 mediates MET-associated stemness in NSCLC, however, remains unknown.

We therefore examined the role of CAV2 in NSCLC stemness and its regulation by MET-associated signaling. We tested whether MET-ERK signaling regulates CAV2 transcription through HIF-1α and whether CAV2 contributes to the self-renewal and tumor-initiating phenotypes induced by MET overexpression. We also assessed whether CAV2 depletion alters the response to crizotinib in vitro and in xenograft models.

2. Materials and methods

Cell culture

Human NSCLC cell lines H1993, EBC-1, H1299, H1975, A549, and PC9 were obtained from Zhejiang Meisen Cell Technology Co., Ltd. (CTCC, Hangzhou, China) or the Cell Bank of the Chinese Academy of Sciences (Shanghai, China). Cell-line identity was confirmed by short tandem repeat profiling before use. Cells were cultured in Dulbecco's modified Eagle medium (DMEM; Gibco, 11965092, Grand Island, NY, USA) supplemented with 10% fetal bovine serum (Gibco, 10099141C), 100 IU/mL penicillin, and 100 μg/mL streptomycin (Gibco, 15140122) at 37°C in a humidified atmosphere containing 5% CO_2. All cell lines were routinely tested and confirmed to be free of mycoplasma.

Patient cohort and assessment of MET copy number

We retrospectively collected 40 archived formalin-fixed, paraffin-embedded NSCLC specimens obtained between 2015 and 2024 from the Department of Pathology, Tongji Hospital, Tongji Medical College, Huazhong University of Science and Technology. Eligible cases had histologically confirmed NSCLC, an available diagnostic MET fluorescence in situ hybridization (FISH) result in the hospital electronic medical record or pathology information system, sufficient viable tumor tissue for immunohistochemistry, and the clinicopathological information required for this study. Cases with insufficient or poorly preserved tumor tissue, technically uninterpretable or equivocal FISH results, or duplicate specimens from the same patient were excluded. The cohort comprised 20 MET-FISH-positive and 20 MET-FISH-negative cases.

MET copy-number results were obtained from finalized clinical pathology reports. FISH had been performed by the hospital pathology laboratory during routine diagnostic evaluation and was not repeated by the research investigators. Cases with an average MET gene copy number of at least 5 signals per tumor nucleus (MET GCN ≥ 5) were classified as MET-FISH-positive; cases below this threshold were classified as MET-FISH-negative. Because FISH was performed directly on FFPE tissue sections, no extracted DNA was used. Only cases with definitive and technically evaluable FISH results were included.

Immunohistochemical evaluation

MET and CAV2 immunohistochemical staining was evaluated on serial FFPE sections. Two pathologists, blinded to the FISH classification, independently assessed staining intensity and the proportion of positive tumor cells. Discrepant assessments were adjudicated by a third pathologist. H-scores were calculated by multiplying the staining intensity score (0–3) by the percentage of positive tumor cells, producing a score from 0 to 300.

RNA isolation and quantitative real-time PCR (qRT-PCR)

Total RNA was isolated using the RNeasy Mini Kit (Qiagen, 74104, Hilden, Germany). Complementary DNA was synthesized from 1 μg of total RNA using the PrimeScript RT Reagent Kit (Takara, RR037A, Shiga, Japan). Quantitative real-time PCR was performed with TB Green Premix Ex Taq II (Takara, RR820A) on a CFX96 Real-Time PCR Detection System (Bio-Rad, Hercules, CA, USA). Relative mRNA expression was normalized to GAPDH and calculated using the 2^−ΔΔCt method. Primer sequences are provided in Supplementary Table 1.

Plasmid transfection, siRNA transfection and lentiviral infection

Lentiviral vectors encoding human MET or the corresponding empty-vector control were purchased from Jikai Gene (Shanghai, China). Lentiviral vectors expressing CAV2-targeting short hairpin RNAs (CAV2sh) or a non-targeting control (shCtrl) were obtained from Obio Technology (Shanghai, China). Cells were infected in the presence of polybrene (Sigma-Aldrich, P4707, St. Louis, MO, USA) and selected with

puromycin (2 μg/mL) for 7 days. For transient HIF1A overexpression, cells were transfected with a HIF1A expression plasmid or empty vector using Lipofectamine 3000 (Invitrogen, L3000015, Carlsbad, CA, USA). Small interfering RNAs targeting MET or HIF1A and a non-targeting control siRNA were synthesized by Tongyong Technology (Anhui, China) and transfected using Lipofectamine RNAiMAX (Invitrogen, 13778075). Cells were collected 48–72 h after transfection. Overexpression and knockdown were confirmed by qRT-PCR and western blotting.

Western blots

Cells were lysed in RIPA buffer (Beyotime, P0013B, Shanghai, China) supplemented with protease and phosphatase inhibitor cocktails (MedChemExpress, HY-K0010 and HY-K0021, Monmouth Junction, NJ, USA). Protein concentrations were measured using a BCA Protein Assay Kit (Thermo Fisher Scientific, 23225, Rockford, IL, USA).

Equal amounts of protein (20–40 μg) were separated by SDS-PAGE and transferred to polyvinylidene fluoride membranes (Millipore, IPVH00010, Billerica, MA, USA). Membranes were blocked with 5% non-fat milk in TBST for 1 h at room temperature and incubated with primary antibodies overnight at 4°C. After washing, membranes were incubated with horseradish peroxidase-conjugated secondary antibodies for 1 h at room temperature. Bands were visualized using enhanced chemiluminescence reagents (Bio-Rad, 1705061) on a ChemiDoc Imaging System (Bio-Rad). Band intensities were quantified using ImageJ and normalized to β-tubulin or GAPDH. Primary antibodies are listed in Supplementary Table 2.

RNA sequencing

Total RNA from H1993 cells was isolated using the RNeasy Mini Kit (Qiagen, 74104). RNA quality assessment, library preparation, and high-throughput sequencing on an Illumina NovaSeq 6000 platform were performed as fee-for-service technical support by Tsingke Biotechnology Co., Ltd. (Beijing, China). The raw sequencing data were returned to the authors, who performed quality control, alignment to the human reference genome, differential expression analysis using DESeq2, and gene set enrichment analysis using the Hallmark, KEGG, and Reactome gene sets. The authors were responsible for data interpretation.

Dual-luciferase reporter assays

H1993 cells were seeded in 96-well plates at 1.5×10^4 cells per well and transfected with Lipofectamine 2000 (Thermo Fisher Scientific) at a final concentration of 2 μg/mL. Each well received a HIF1A expression vector (100 ng), a wild-type or mutant CAV2 promoter luciferase reporter (80 ng), and the pRL-TK Renilla luciferase plasmid (10 ng; Promega, Madison, WI, USA). Luciferase activity was measured 24 h after transfection using the Dual-Luciferase Reporter Assay System (Promega, E1960) according to the manufacturer's instructions.

Chromatin immunoprecipitation (ChIP)

Chromatin immunoprecipitation (ChIP) assays were performed as follows. Cells were cross-linked with formaldehyde, and the reaction was quenched with glycine. Nuclei were isolated, and chromatin was sheared into 300-700-bp fragments using a Covaris S200 sonicator. Fragment size was verified using D1000 ScreenTape on an Agilent TapeStation. Equal amounts of chromatin were incubated overnight at 4°C with the indicated antibody or control IgG, followed by capture with protein A/G magnetic beads. After sequential washing, immune complexes were eluted and cross-links were reversed. DNA was purified using spin-column PCR purification kits and analyzed by qPCR with primers targeting the putative R1 and R2 binding regions. Ten percent of the input chromatin was processed in parallel for normalization. Enrichment was calculated using the percentage-input method.

Animal experiments

All animal experiments were approved by the Institutional Animal Care and Use Committee of Huazhong University of Science and Technology (approval no. 386-20231211; 1 February 2024). Female BALB/c nude mice, 5 weeks of age and weighing 20–22 g, were obtained from GemPharmatech Co., Ltd. and housed under specific pathogen-free conditions.

H1993 cells stably expressing a non-targeting control shRNA or CAV2-targeting shRNA were suspended at 5 × 10^6 cells in 100 µL of a 1:1 mixture of cell suspension and Matrigel and injected subcutaneously into the left axilla. Because the two cell populations were established before implantation, randomization was performed separately within each cell-line cohort. Approximately 14 days after implantation, when individual tumors reached 50–100 mm^3, eligible mice in each cohort were randomly assigned by a random-number table to vehicle or crizotinib treatment. The four resulting groups were control plus vehicle, CAV2sh plus vehicle, control plus crizotinib, and CAV2sh plus crizotinib (n = 8 per group; 32 mice in total).

Crizotinib was administered by oral gavage at 50 mg/kg once daily for 30 days. The formulation contained 10% DMSO, 40% PEG300, 5% Tween 80, and 45% saline. Vehicle-treated mice received an equivalent volume of the corresponding vehicle. Tumor length and width were measured with calipers at treatment initiation (day 0) and every 3 days thereafter. Day-0 measurements represent actual tumor volumes at treatment initiation and were not baseline-subtracted.

$$\mathrm{Tumor\ volume} = \frac{\mathrm{length} \times \mathrm{width}^2}{2}.$$

Mice were euthanized on treatment day 30 or earlier if a predefined humane endpoint was reached. Tumors were excised, photographed, and weighed. Each mouse was treated as one independent experimental unit.

Prospectively defined humane endpoints included a tumor approaching but not exceeding 2,000 mm^3; tumor ulceration, necrosis, or infection; interference with movement, feeding, or drinking; marked body-weight loss; persistent pain or distress; or substantial deterioration in general condition. Tumor

measurements were reviewed at each assessment to ensure that tumor burden remained below 2,000 mm^3. Mice were euthanized by gradual-fill CO_2 inhalation followed by cervical dislocation. Animal identification and treatment allocation were performed by an investigator who was not involved in tumor measurement, sample collection, or data analysis. No animals or data points were excluded. Experiments were conducted and reported in accordance with ARRIVE 2.0 guidelines.

Limiting dilution xenograft assays

Limiting dilution xenograft assays were performed in female BALB/c nude mice. Cells were resuspended in a 1:1 mixture of cell suspension and Matrigel and injected subcutaneously into the left axilla in a final volume of 100 μL.

For the CAV2 loss-of-function experiment, H1993 cells expressing scrambled control shRNA or CAV2-targeting shRNA were injected at 2×10^6, 1×10^6, or 5×10^5 cells per mouse. Each group included 10 mice at each cell dose. Tumor formation was monitored for 30 days after transplantation, and tumor incidence was recorded at each dose.

For the MET epistasis experiment, control cells, MET-overexpressing cells, and MET-overexpressing cells with CAV2 knockdown were injected at 1×10^6, 5×10^5, or 2×10^5 cells per mouse. Each group included eight mice at each cell dose. Tumor formation was monitored for 30 days after transplantation, and tumor incidence was recorded for each group and dose.

Tumor-initiating cell frequencies and 95% confidence intervals were estimated by extreme limiting dilution analysis (ELDA). Differences in tumor-initiating cell frequency were assessed using the ELDA software package. Mice were euthanized at the end of the observation period or earlier if a predefined humane endpoint was reached. Each mouse was treated as one independent experimental unit.

Survival analysis

Survival analyses were performed using the Kaplan-Meier Plotter platform (www.kmplot.com/analysis) in an independent public NSCLC cohort. Patients were divided into high- and low-CAV2-expression groups using the median expression level as the cutoff. Overall survival and progression-free survival were estimated by the Kaplan-Meier method, and groups were compared using the log-rank test. Hazard ratios and 95% confidence intervals were obtained from the platform.

Statistical analysis

Data are presented as mean ± SD. Normality was assessed using the Kolmogorov-Smirnov test. Student's t test, the Mann-Whitney U test, or one-way analysis of variance with Bonferroni correction was used as appropriate. Tumor growth curves were analyzed by two-way repeated-measures analysis of variance followed by Bonferroni-adjusted comparisons between the indicated groups. Endpoint tumor weights were analyzed by one-way analysis of variance followed by Bonferroni's multiple-comparisons test. The prespecified comparisons of primary interest were the combination group versus CAV2sh alone

and the combination group versus crizotinib alone. Each mouse was an independent experimental unit, with eight mice per group. Analyses were performed using GraphPad Prism version 9.3 (GraphPad Software, La Jolla, CA, USA). A two-sided P value < 0.05 was considered statistically significant.

3. Results

3.1 CAV2 expression is associated with MET amplification in NSCLC

MET amplification is a well-established oncogenic alteration in non-small cell lung cancer (NSCLC). Patients with MET-amplified tumors often exhibit aggressive clinical behavior and may eventually develop resistance to MET-targeted therapies[27–29]. To identify genes associated with MET-amplified NSCLC, we integrated expression data from the TCGA-LUAD, TCGA-LUSC, and CCLE datasets. Spearman correlation analyses identified genes consistently associated with MET expression across datasets (Fig. 1A). CAV2 was among the reproducible candidates and was highly expressed in the MET-amplified NSCLC cell lines EBC-1 and H1993 (Fig. S1A). MET and CAV2 expression correlated positively across the analyzed datasets ($r = 0.56$, $P < 0.01$; Fig. 1B). Their genomic copy-number alterations were also positively associated (Fig. 1C).

We then examined 40 archived NSCLC specimens from the Department of Pathology, Tongji Hospital. Based on clinical FISH reports and a cutoff of MET GCN ≥ 5, 20 tumors were classified as MET-FISH-positive and 20 as MET-FISH-negative. CAV2 H-scores were higher in MET-FISH-positive tumors (Fig. 1D, E), and MET and CAV2 H-scores correlated across individual specimens (Spearman's $\rho = 0.41$, $P = 0.0009$; Fig. 1F). CAV2 copy-number data were unavailable for this cohort. The observed association therefore cannot be separated from potential regional co-amplification of MET and CAV2 at 7q31.2 and does not establish direct regulation in patient tumors. In an independent public NSCLC cohort, high CAV2 expression was associated with shorter overall survival (HR = 1.25, 95% CI 1.11–1.41, $P = 0.00024$) and progression-free survival (HR = 1.46, 95% CI 1.23–1.73, $P = 1 \times 10^{-5}$; Fig. 1G, H).

Figure 1. CAV2 expression is associated with MET status in NSCLC and with poorer survival in an independent public cohort.

(A) Integrated co-expression analysis of TCGA-LUAD, TCGA-LUSC, and CCLE datasets identified genes consistently associated with MET expression. (B) Correlation between MET and CAV2 expression. (C) Correlation between MET and CAV2 genomic copy-number alterations in NSCLC datasets. (D) Representative MET and CAV2 immunohistochemical staining in MET-FISH-negative and MET-FISH-positive NSCLC specimens. Scale bars, 200 μm. (E) CAV2 H-scores in MET-FISH-negative and MET-FISH-positive specimens. (F) Correlation between MET and CAV2 H-scores. The fitted line and Spearman correlation statistics are shown. (G, H) Kaplan-Meier analyses of overall survival and progression-free survival according to CAV2 expression in an independent public NSCLC cohort. Data are presented as

mean ± SD where applicable. Statistical significance was assessed using Student's t test, Spearman correlation analysis, or the log-rank test, as appropriate. *P < 0.05; **P < 0.01.

3.2 CAV2 maintains stem-like phenotypes in NSCLC

Given that aberrant MET activation has been closely linked to cancer stem-like phenotypes and therapeutic resistance in NSCLC, and considering recent evidence implicating CAV2 in the regulation of cancer stemness-associated programs, we next sought to determine whether CAV2 functionally contributes to the maintenance of stem-like properties in NSCLC[26, 30]. We examined CAV2 function in EBC-1 and H1993 cells, two MET-amplified NSCLC models with constitutive MET activation [31–33]. Genomic copy-number analysis confirmed MET amplification in both lines relative to non-MET-amplified PC9 cells (Fig. S2A). Two independent shRNAs reduced CAV2 mRNA and protein expression (Fig. 2A-C). CAV2 depletion delayed wound closure and reduced migration and invasion in both cell lines (Fig. S2B-I). It also reduced tumorsphere diameter, number, and formation efficiency (Fig. 2D-F; Fig. S3A, B). Flow cytometry showed lower CD44 fluorescence after CAV2 depletion (Fig. 2G, H; Fig. S3C), and ALDH1A1, OCT4, and NANOG expression decreased at the protein and mRNA levels (Fig. 2I, J; Fig. S3D, E). In limiting dilution xenograft assays, CAV2-depleted H1993 cells formed fewer tumors at limiting cell doses (Fig. 2K, L). ELDA estimated a lower tumor-initiating cell frequency in the CAV2sh group than in controls (Fig. 2M, N). Re-expression of CAV2 in CAV2-depleted cells restored CAV2 protein levels and tumorsphere formation (Fig. 2O, P; Fig. S3F-I). Together, these results show that CAV2 contributes to stemness-associated phenotypes and tumor initiation in the tested MET-amplified NSCLC models.

RNA sequencing was performed in H1993 cells to examine transcriptional changes after CAV2 depletion. Differentially expressed genes are shown in the volcano plot and heatmap (Fig. S4A, B). Exploratory GSEA indicated negative enrichment trends for WNT, Hedgehog, and TGF-β signaling, although none reached statistical significance (Fig. S4C-E).

(A-C) CAV2 knockdown in EBC-1 and H1993 cells was confirmed by qRT-PCR and western blotting. Full-length blots are shown in Supplementary Material 3, Fig. 1A. (D) Representative tumorspheres formed by control and CAV2-depleted cells. (E, F) Average tumorsphere diameter in H1993 and EBC-1 cells, respectively. (G, H) Representative flow cytometric histograms of CD44 expression in H1993 and EBC-1 cells. (I, J) Western blot analysis of ALDH1A1, OCT4, and NANOG after CAV2 depletion. Full-length blots are shown in Supplementary Material 3, Fig. 1B. (K) Representative tumors from the limiting dilution assay. (L) Tumor incidence at each cell dose. (M, N) ELDA estimates of tumor-initiating cell frequency. Control and CAV2-depleted H1993 cells were injected at 2×10^6, 1×10^6, or 5×10^5 cells per mouse in 100 μL of a 1:1 cell suspension and Matrigel mixture. Tumor formation was monitored for 30 days, with 10 mice per group at each dose. (O) Western blot confirmation of CAV2 re-expression. Full-length blots are shown in Supplementary Material 3, Fig. 1C. (P) Representative tumorspheres after CAV2 re-expression.

Data are presented as mean ± SD from at least three independent experiments. Statistical significance was assessed using Student's t test or one-way analysis of variance, as appropriate. *P < 0.05; **P < 0.01;

***P < 0.001.

3.3 CAV2 expression is regulated by MET-associated signaling in NSCLC

CAV2 protein expression was higher in the MET-amplified cell lines H1993 and EBC-1 than in PC9, H1975, A549, and H1299 cells (Fig. 3A; Fig. S5A, B). HGF stimulation increased CAV2 expression in a dose-dependent manner and activated MET signaling in H1993 and EBC-1 cells (Fig. 3B, C; Fig. S5C, D). Crizotinib treatment reduced CAV2 expression both with and without HGF stimulation (Fig. 3D-G; Fig. S5E, F). Genetic manipulation produced consistent results: MET knockdown reduced CAV2 expression, whereas MET overexpression increased it (Fig. 3H-K; Fig. S5G-J). These pharmacological and genetic findings support regulation of CAV2 expression by MET-associated signaling in the tested NSCLC models.

(A) Basal CAV2 protein expression in NSCLC cell lines with different MET activation states. Full-length blots are shown in Supplementary Material 3, Fig. 2A. (B, C) HGF stimulation increased CAV2 expression in H1993 and EBC-1 cells. Full-length blots are shown in Supplementary Material 3, Fig. 2B. (D-G) Crizotinib treatment reduced CAV2 expression with or without HGF stimulation. Full-length blots are shown in Supplementary Material 3, Figs. 3 and 4A. (H, I) MET knockdown reduced CAV2 expression. Full-length blots are shown in Supplementary Material 3, Fig. 4B. (J, K) MET overexpression increased CAV2 expression. Full-length blots are shown in Supplementary Material 3, Fig. 4C, D. Data are presented as mean ± SD from at least three independent experiments. Statistical significance was assessed using Student's t test or one-way analysis of variance, as appropriate. *P < 0.05; **P < 0.01; ***P < 0.001.

3.4 MET-associated signaling regulates CAV2 transcription through ERK and HIF1A

These findings established CAV2 as a downstream effector of oncogenic MET signaling. Given that MET activates multiple intracellular signaling cascades, including the MAPK/ERK and PI3K/AKT pathways, we next sought to determine which pathway mediates CAV2 expression. Among the major downstream effectors of MET, both MAPK/ERK and PI3K/AKT signaling have been extensively implicated in the regulation of transcriptional programs associated with tumor progression and cancer stemness[34–36]. To determine which MET-associated pathway regulates CAV2, we treated H1993 and EBC-1 cells with the MEK inhibitor U0126 or the PI3K inhibitor LY294002. U0126 reduced ERK phosphorylation and CAV2 protein expression, whereas LY294002 inhibited AKT phosphorylation with little effect on CAV2 (Fig. 4A-D). U0126 also reduced CAV2 mRNA in a dose-dependent manner (Fig. 4E, F) and decreased CAV2 expression over time (Fig. S6A, B). These results implicate the MEK-ERK pathway in the regulation of CAV2 expression. Because ERK regulates transcription through downstream effectors rather than direct DNA binding [38], we next examined candidate transcription factors linking ERK signaling to the CAV2 promoter.

PROMO and JASPAR analyses identified several candidate transcription-factor binding motifs in the CAV2 promoter. We focused on HIF1A because it can act downstream of receptor tyrosine kinase and ERK signaling [37–39]. U0126 reduced HIF-1α expression (Fig. S6C, D), and MET knockdown produced a similar reduction (Fig. S6E, F). HIF1A knockdown decreased CAV2 expression, whereas HIF1A overexpression increased it in both H1993 and EBC-1 cells (Fig. 4G-N). These results place HIF1A downstream of MET-ERK signaling and support its involvement in CAV2 regulation.

We cloned an approximately 2-kb region upstream of the CAV2 transcription start site into a pGL3-basic luciferase reporter. MET knockdown reduced CAV2 promoter activity, whereas HIF1A overexpression increased it and partially restored promoter activity in MET-depleted cells (Fig. 4O). Two predicted HIF-1α-binding motifs were located at − 1335 to − 1326 bp (R1) and − 289 to − 280 bp (R2) relative to the transcription start site (Fig. 4P, Q). Mutation of R2, but not R1, attenuated HIF1A-induced promoter activity (Fig. 4R). ChIP-qPCR further showed HIF-1α enrichment at the R2-containing promoter region (Fig. 4S). These findings support direct HIF-1α occupancy of the CAV2 promoter and identify R2 as the principal responsive element in the reporter system.

(A-D) Western blot analysis of CAV2 and pathway activation in H1993 and EBC-1 cells treated with U0126 or LY294002. Full-length blots are shown in Supplementary Material 3, Fig. 5A, B. (E, F) CAV2 mRNA expression after treatment with increasing concentrations of U0126. (G-J) CAV2 expression after HIF1A knockdown. Full-length blots are shown in Supplementary Material 3, Fig. 5E. (K-N) CAV2 expression after HIF1A overexpression. Full-length blots are shown in Supplementary Material 3, Fig. 5F. (O) Effects of MET knockdown and HIF1A overexpression on CAV2 promoter activity. (P) Sequence logo of the predicted HIF-1α-binding motif. (Q) Wild-type and mutant CAV2 promoter reporter constructs. (R) Effects of HIF1A overexpression on wild-type and mutant promoter reporters. (S) ChIP-qPCR analysis of HIF-1α occupancy at the CAV2 promoter. Data are presented as mean ± SD from three independent experiments. Statistical significance was assessed using Student's t test or one-way analysis of variance with the indicated post hoc analysis. *P < 0.05; **P < 0.01; ***P < 0.001.

3.5 CAV2 contributes to MET-induced stemness in NSCLC

We next examined whether CAV2 contributes to the stemness-promoting effects of MET overexpression. H1993 cells were engineered to overexpress MET with or without concurrent CAV2 knockdown. Western blotting and qRT-PCR confirmed the expected changes in MET and CAV2 expression (Fig. 5A-C).

MET overexpression increased tumorsphere diameter and formation efficiency, whereas concurrent CAV2 knockdown attenuated these changes (Fig. 5D-F). In limiting dilution xenograft assays, MET-overexpressing cells formed tumors more frequently than control cells, and CAV2 knockdown reduced this increase (Fig. 5G-I). ELDA likewise showed that the higher tumor-initiating cell frequency associated with MET overexpression was reduced by CAV2 depletion (Fig. 5J, K). These findings support CAV2 as a downstream mediator that contributes to the self-renewal and tumor-initiating phenotypes induced by MET overexpression in the tested NSCLC model.

(A) Western blot confirmation of MET overexpression and CAV2 knockdown. Full-length blots are shown in Supplementary Material 3, Fig. 6A. (B, C) qRT-PCR analysis of MET and CAV2 expression. (D) Representative tumorspheres formed by control, MET-overexpressing, and MET-overexpressing/CAV2-depleted cells. (E) Average tumorsphere diameter. (F) Tumorsphere formation efficiency. (G) Schematic of the limiting dilution xenograft assay. (H) Representative tumors at each cell dose. (I) Tumor incidence. (J, K) ELDA estimates of tumor-initiating cell frequency. Control, MET-overexpressing, and MET-overexpressing/CAV2-depleted cells were injected at 1×10^6, 5×10^5, or 2×10^5 cells per mouse in 100 μL of a 1:1 cell suspension and Matrigel mixture. Tumor formation was monitored for 30 days, with eight mice per group at each dose. Data are presented as mean ± SD from three independent experiments. Statistical significance was assessed using Student's t test or one-way analysis of variance with the indicated post hoc analysis. ELDA statistics were calculated using the ELDA software package. *P < 0.05; **P < 0.01; ***P < 0.001.

3.6 CAV2 depletion increases the response to crizotinib in MET-amplified NSCLC models

CAV2 depletion shifted the crizotinib dose-response curve to the left, reducing the IC_{50} from 3.49 μM in control H1993 cells to 0.623 μM in CAV2sh cells (Fig. 6A). We then evaluated CAV2 depletion and crizotinib treatment in xenograft models. Mice were assigned to vehicle or crizotinib within each cell-line cohort when individual tumors reached 50–100 mm^3, and tumor burden was monitored for 30 days. The combination group had the lowest endpoint tumor weight, which was significantly lower than that of either monotherapy group (Fig. 6B, C). Tumor volumes were also lowest in the combination group during the later treatment period and on day 30 (Fig. 6D). Thus, combined CAV2 depletion and crizotinib treatment suppressed tumor growth more than either intervention alone in this xenograft model.

Figure 6. CAV2 depletion increases the response to crizotinib in MET-amplified NSCLC models.

(A) Crizotinib dose-response curves in control and CAV2-depleted H1993 cells. Cell viability was normalized to the untreated condition, and nonlinear regression was used to estimate IC_{50} values (control, 3.49 μM; CAV2sh, 0.623 μM). (B) Excised xenograft tumors after 30 days of vehicle or crizotinib treatment. Rows represent control plus vehicle, CAV2sh plus vehicle, control plus crizotinib, and CAV2sh plus crizotinib; n = 8 mice per group. (C) Endpoint tumor weights. Each point represents one mouse; bars and error bars indicate mean ± SD. (D) Tumor volumes measured at treatment initiation and every 3 days for 30 days. Data are mean ± SD; n = 8 per group. Treatment began when individual tumors measured 50–100 mm^3, and tumor burden remained below the prespecified humane endpoint of 2,000 mm^3. Tumor weights were analyzed by one-way analysis of variance with Bonferroni's multiple-comparisons test. Tumor growth curves were analyzed by two-way repeated-measures analysis of variance followed by Bonferroni-adjusted comparisons. **P < 0.01; ***P < 0.001; ns, not significant.

4. Discussion

This study identifies CAV2 as a mediator of MET-associated stemness phenotypes in experimental NSCLC models. MET-FISH-positive patient tumors had higher CAV2 H-scores than MET-FISH-negative tumors, although regional co-amplification at 7q31.2 remains a potential explanation for this association. Functional studies showed that CAV2 supports self-renewal and tumor initiation, while mechanistic experiments linked CAV2 transcription to MET-associated ERK-HIF1A signaling.

MET amplification is an important oncogenic alteration in NSCLC and is associated with tumor progression and adverse clinical outcomes [27–29, 40].. Its role in maintaining stem-like cellular states is less well defined. In our experimental models, CAV2 depletion reduced tumorsphere formation, stemness-associated marker expression, and tumor-initiating capacity. MET overexpression enhanced self-renewal and tumor formation, and both effects were attenuated by CAV2 knockdown. These data connect MET-associated signaling with a CAV2-dependent program that contributes to tumor cell plasticity.

CAV2 is a component of caveolae, membrane domains that regulate receptor trafficking, signal compartmentalization, cytoskeletal organization, and communication with the cellular environment [19–21]. Its role in cancer varies by context, and it has received less attention than CAV1. Our results extend previous reports linking CAV2 to aggressive tumor behavior and stem-like phenotypes [23–26]. The present data do not establish how CAV2 acts at the membrane, but its known functions raise the possibility that it influences the duration or localization of receptor tyrosine kinase signaling. This possibility and the reported roles of CAV2 in metabolism and mitochondrial function require direct investigation in MET-amplified NSCLC.

Our mechanistic data identify ERK and HIF1A as regulators of CAV2 transcription. MEK inhibition reduced CAV2 expression, whereas PI3K inhibition had little effect under the conditions tested. HIF1A knockdown and overexpression produced corresponding changes in CAV2, and promoter assays identified R2 as the main HIF1A-responsive element. ChIP-qPCR confirmed HIF-1α occupancy at the R2-containing region. These findings link MET-associated signaling to CAV2 transcription through ERK and HIF1A. They also extend the role of HIF-1α beyond hypoxic responses, consistent with evidence that oncogenic signaling can regulate HIF-1α under non-hypoxic conditions [37, 41–46].

The patient-tissue analysis has an important genomic limitation. MET and CAV2 are both located at chromosome 7q31.2, so higher CAV2 expression in MET-FISH-positive tumors may partly reflect regional co-amplification rather than an independent consequence of MET signaling. CAV2 copy-number data were unavailable, precluding multivariable or partial-correlation analyses that adjusted for CAV2 genomic dosage. The cohort also lacked complete follow-up; therefore, the survival analyses were performed in an independent public cohort and should not be attributed to the 40 clinical specimens. Studies with paired MET and CAV2 copy-number measurements are needed to determine whether their expression association persists after adjustment for regional co-amplification.

The findings may also have therapeutic implications. Cancer stem-like cells can persist during targeted treatment and contribute to tumor regrowth [47, 48]. In our models, CAV2 depletion increased the

response to crizotinib in vitro and reduced tumor burden when combined with crizotinib in vivo. These results do not establish acquired drug resistance, but they suggest that CAV2-dependent stemness may influence the treatment response of MET-amplified NSCLC cells.

Direct pharmacological inhibition of CAV2 is not currently available. Future studies could instead examine CAV2-regulated pathways, caveolae-associated signaling complexes, or other components of the MET-ERK-HIF1A-CAV2 pathway. Such studies should use clinically relevant MET inhibitors and patient-derived models to determine whether the experimental effects observed here translate to therapeutic benefit. The value of CAV2 as a predictive biomarker also requires validation in prospective cohorts with documented treatment and follow-up data.

Several additional limitations should be considered. The clinical cohort was small and retrospective, and the functional studies relied mainly on established cell lines and xenografts. Patient-derived organoids, patient-derived xenografts, and genetically engineered models will be needed to test the generalizability of the findings. Additional transcription factors or chromatin regulators may cooperate with HIF-1α at the CAV2 promoter. Finally, the current models do not capture the full tumor microenvironment, which can influence stemness, drug response, and communication among tumor, stromal, immune, and vascular cells.

5. Conclusions

MET-associated signaling promotes CAV2 expression and stemness-related phenotypes in experimental NSCLC models. CAV2 depletion reduced self-renewal and tumor initiation and increased the antitumor effect of crizotinib. In patient specimens, MET-FISH positivity was associated with higher CAV2 expression, although regional co-amplification at 7q31.2 may contribute to this relationship. CAV2 is therefore a candidate MET-associated biomarker and experimental therapeutic vulnerability that requires validation in copy-number-resolved clinical cohorts and patient-derived models.

Abbreviations

FISH
Fluorescence in situ hybridization
FFPE
Formalin-fixed, paraffin-embedded
NSCLC
Non-small cell lung cancer
CAV1
Caveolin-1
CAV2
Caveolin-2
CI

Confidence interval
CSCs
Cancer stem cells
GSEA
Gene set enrichment analysis
EMT
Epithelial-mesenchymal transition
STR
Short tandem repeat
BSA
Bovine serum albumin
PVDF
Polyvinylidene fluoride
ECL
Enhanced chemiluminescence
ChIP
Chromatin immunoprecipitation
HR
Hazard ratio
HGF
Hepatocyte growth factor
ELDA
Extreme limiting dilution analysis
OS
Overall survival
PFS
Progression-free survival

Declarations

Ethics approval and consent to participate

The study was approved by the Ethics Committee of Tongji Hospital, Huazhong University of Science and Technology (approval no. TJ-IRB202404114; 30 April 2024). Archived pathological sections were used for observational analyses, and no additional human samples, interventions, or identifiable personal information were collected. The requirement for written informed consent was waived by the Ethics Committee. H1993 and EBC-1 cells were obtained from Zhejiang Meisen Cell Technology Co., Ltd.; H1299, H1975, A549, and PC9 cells were obtained from the Cell Bank of the Chinese Academy of Sciences, as described in the Methods. The animal study was approved by the Experimental Animal Ethics Committee of Huazhong University of Science and Technology (approval no. 386-20231211; 1

February 2024). Animal experiments were conducted and reported in accordance with ARRIVE 2.0 guidelines. All methods were performed in accordance with relevant guidelines and regulations.

Consent for publication

Not applicable.

Competing interests

The authors declare that they have no competing interests.

Funding

This work was supported by the National Natural Science Foundation of China (grant no. 82172716), the Beijing Xisike Clinical Oncology Research Foundation (grant no. Y-2023AZMETMS-0013), the Hubei Provincial Natural Science Foundation of China (grant no. 2026AFC1314), and the Hubei Chen Xiaoping Science and Technology Development Foundation (grant no. CXPJJH125031-03).

Author Contribution

S.Y. and S.X. conceived and designed the study. S.Y. developed the experimental strategy and supervised the project. J.T., Y.Z., Y.L., Y.F., K.Z., X.L., X.X., Y.H., Z.H., and D.Y. performed the cellular, molecular, and animal experiments. J.T., Y.Z., Y.L., and Y.F. collected experimental and clinical data and performed the bioinformatic and statistical analyses. S.Y., J.T., and Y.Z. analyzed and interpreted the data. S.Y. drafted the manuscript. S.X. acquired funding, supervised the study, and critically revised the manuscript. All authors read and approved the final manuscript and agreed to be accountable for the work.

Acknowledgement

The authors thank members of the Department of Oncology, Tongji Hospital, Tongji Medical College, Huazhong University of Science and Technology, for technical assistance and discussions. The authors also thank the Core Facility of Tongji Hospital for support with imaging, flow cytometry, and animal experiments, and the Department of Pathology for assistance with tissue preparation and immunohistochemical evaluation. RNA quality assessment, library preparation, and high-throughput sequencing were provided as fee-for-service technical support by Tsingke Biotechnology Co., Ltd. The authors performed the biological experiments and downstream bioinformatic analyses and were responsible for data interpretation and the conclusions presented. Artificial intelligence tools were used for grammar checking and language editing during manuscript revision. All AI-assisted text was reviewed, verified, and edited by the authors, who take full responsibility for the final manuscript.

Data Availability

The public datasets analyzed in this study are available from The Cancer Genome Atlas (TCGA-LUAD and TCGA-LUSC; https://portal.gdc.cancer.gov/), the Cancer Cell Line Encyclopedia (https://portals.broadinstitute.org/ccle), the JASPAR database (http://jaspar.genereg.net/), and the Kaplan-Meier Plotter platform (https://kmplot.com/). RNA-seq raw count data supporting the findings are provided in Supplementary Material 2.

References

1. P. Dalerba, S.J. Dylla, I.K. Park, R. Liu, X. Wang, R.W. Cho, T. Hoey, A. Gurney, E.H. Huang, D.M. Simeone et al., Phenotypic characterization of human colorectal cancer stem cells. Proc. Natl. Acad. Sci. U.S.A. **104**(24), 10158–10163 (2007)
2. L. Ricci-Vitiani, D.G. Lombardi, E. Pilozzi, M. Biffoni, M. Todaro, C. Peschle, De R. Maria, Identification and expansion of human colon-cancer-initiating cells. Nature. **445**(7123), 111–115 (2007)
3. T. Huang, X. Song, D. Xu, D. Tiek, A. Goenka, B. Wu, N. Sastry, B. Hu, S.Y. Cheng, Stem cell programs in cancer initiation, progression, and therapy resistance. Theranostics. **10**(19), 8721–8743 (2020)
4. H. Lee, B. Kim, J. Park, S. Park, G. Yoo, S. Yum, W. Kang, J.M. Lee, H. Youn, B. Youn, Cancer stem cells: landscape, challenges and emerging therapeutic innovations. Signal. Transduct. Target. therapy. **10**(1), 248 (2025)
5. S. Cai, N. Li, X. Bai, L. Liu, A. Banerjee, K. Lavudi, X. Zhang, J. Zhao, M. Venere, W. Duan et al., ERK inactivation enhances stemness of NSCLC cells via promoting Slug-mediated epithelial-to-mesenchymal transition. Theranostics. **12**(16), 7051–7066 (2022)
6. J. Fu, X. Su, Z. Li, L. Deng, X. Liu, X. Feng, J. Peng, HGF/c-MET pathway in cancer: from molecular characterization to clinical evidence. Oncogene. **40**(28), 4625–4651 (2021)
7. M. Park, M. Dean, K. Kaul, M.J. Braun, M.A. Gonda, G. Vande Woude, Sequence of MET protooncogene cDNA has features characteristic of the tyrosine kinase family of growth-factor receptors. Proc. Natl. Acad. Sci. U.S.A. **84**(18), 6379–6383 (1987)
8. P. Goleij, M.M. Heidari, H. Motevalli, S. Abolfazli, M.A. Khazeei Tabari, A. Rezaee, S.L. D, M. Daglia, M. Aschner, H. Khan, Targeting the HGF/MET axis in cancer: therapeutic promise for natural compounds. Eur. J. Med. Chem. **298**, 118027 (2025)
9. N. Puri, S. Ahmed, V. Janamanchi, M. Tretiakova, O. Zumba, T. Krausz, R. Jagadeeswaran, R. Salgia, c-Met is a potentially new therapeutic target for treatment of human melanoma. Clin. cancer research: official J. Am. Association Cancer Res. **13**(7), 2246–2253 (2007)
10. J. Remon, L.E.L. Hendriks, G. Mountzios, R. García-Campelo, S.P.L. Saw, D. Uprety, G. Recondo, G. Villacampa, M. Reck, MET alterations in NSCLC-Current Perspectives and Future Challenges. J. Thorac. oncology: official publication Int. Association Study Lung Cancer. **18**(4), 419–435 (2023)
11. F. Cappuzzo, P.A. Jänne, M. Skokan, G. Finocchiaro, E. Rossi, C. Ligorio, P.A. Zucali, L. Terracciano, L. Toschi, M. Roncalli et al., MET increased gene copy number and primary resistance to gefitinib

therapy in non-small-cell lung cancer patients. Annals oncology: official J. Eur. Soc. Med. Oncol. **20**(2), 298–304 (2009)

12. R. Caparica, C.T. Yen, R. Coudry, S.I. Ou, M. Varella-Garcia, D.R. Camidge, de G. Jr. Castro, Responses to Crizotinib Can Occur in High-Level MET-Amplified Non-Small Cell Lung Cancer Independent of MET Exon 14 Alterations. J. Thorac. oncology: official publication Int. Association Study Lung Cancer. **12**(1), 141–144 (2017)
13. F. Deng, W. Ma, S. Wei, Targeting Mesenchymal-Epidermal Transition (MET) Aberrations in Non-Small Cell Lung Cancer: Current Challenges and Therapeutic Advances. Cancers 2026, **18**(2)
14. C.A. Febres-Aldana, M. Vojnic, I. Odintsov, T. Zhang, R. Cheng, C.Z. Beach, D. Lu, M.S. Mattar, A.M. Gazzo, L. Gili et al., Pan-Cancer Analysis of Oncogenic MET Fusions Reveals Distinct Pathogenomic Subsets with Differential Sensitivity to MET-Targeted Therapy. Cancer Discov. **15**(6), 1141–1158 (2025)
15. V. Cepero, J.R. Sierra, S. Corso, E. Ghiso, L. Casorzo, T. Perera, P.M. Comoglio, S. Giordano, MET and KRAS gene amplification mediates acquired resistance to MET tyrosine kinase inhibitors. Cancer Res. **70**(19), 7580–7590 (2010)
16. Y.R. Choi, M. Hwang, J. Kim, S.Y. Park, S. Kim, J.J. Song, Y. Lee, Overcoming MET-targeted drug resistance in MET-amplified lung cancer by aurora kinase B inhibition. Biochim. et Biophys. acta Mol. cell. Res. **1872**(7), 120001 (2025)
17. L. Cao, Y. Xu, Y. Hu, X. Huang, F. Fu, S. Zhan, L. Huang, Y. Feng, Y. Irene, H. Li et al., Identification of c-Met on Tumor Cells as a Novel Receptor for B7-H3 Entails Implications for Cancer Cell Stemness and Targeted Therapy. *MedComm* 2025, 6(9):e70332
18. S. Gallo, C.B. Folco, T. Crepaldi, The MET Oncogene: An Update on Targeting Strategies. Pharmaceuticals (Basel Switzerland) 2024, **17**(11)
19. L.A. Carver, J.E. Schnitzer, Caveolae: mining little caves for new cancer targets. Nat. Rev. Cancer. **3**(8), 571–581 (2003)
20. R.G. Parton, Caveolae: Structure, Function, and Relationship to Disease. Annu. Rev. Cell Dev. Biol. **34**, 111–136 (2018)
21. D.M. Stea, A. D'Alessio, Caveolae: Metabolic Platforms at the Crossroads of Health and Disease. Int. J. Mol. Sci. 2025, **26**(7)
22. X. Gu, A.M. Reagan, M.E. McClellan, M.H. Elliott, Caveolins and caveolae in ocular physiology and pathophysiology. Prog. Retin. Eye Res. **56**, 84–106 (2017)
23. T. Ando, H. Ishiguro, M. Kimura, A. Mitsui, Y. Mori, N. Sugito, K. Tomoda, R. Mori, K. Harada, T. Katada et al., The overexpression of caveolin-1 and caveolin-2 correlates with a poor prognosis and tumor progression in esophageal squamous cell carcinoma. Oncol. Rep. **18**(3), 601–609 (2007)
24. Y. Zhu, J. Tian, X. Peng, X. Wang, N. Yang, P. Ying, H. Wang, B. Li, Y. Li, M. Zhang et al., A genetic variant conferred high expression of CAV2 promotes pancreatic cancer progression and associates with poor prognosis. *European journal of cancer (Oxford, England*: 1990) 2021, 151:94–105

25. H. Wikman, J.K. Seppänen, V.K. Sarhadi, E. Kettunen, K. Salmenkivi, E. Kuosma, K. Vainio-Siukola, B. Nagy, A. Karjalainen, T. Sioris et al., Caveolins as tumour markers in lung cancer detected by combined use of cDNA and tissue microarrays. J. Pathol. **203**(1), 584–593 (2004)
26. Z. Zhang, C. Wang, Z. Sun, X. Shi, Y. Shuai, Y. Wang, Y. Wang, H. Guo, R. Liu, J. Luo, CAV2-expressing nerves induce metabolic switch toward mitochondrial oxidative phosphorylation to promote cancer stemness. Nat. Commun. **17**(1), 203 (2025)
27. L. Faoro, G.M. Cervantes, E. El-Hashani, R. Salgia, MET receptor tyrosine kinase. J. Thorac. oncology: official publication Int. Association Study Lung Cancer. **4**(11 Suppl 3), S1064–1065 (2009)
28. K. Tsuta, Y. Kozu, T. Mimae, A. Yoshida, T. Kohno, I. Sekine, T. Tamura, H. Asamura, K. Furuta, H. Tsuda, c-MET/phospho-MET protein expression and MET gene copy number in non-small cell lung carcinomas. J. Thorac. oncology: official publication Int. Association Study Lung Cancer. **7**(2), 331–339 (2012)
29. H. Feng, Y. Xia, W. Wang, C. Xu, Q. Wang, Z. Song, Z. Li, J. Yu, W. Zhong, Z. Wang et al., Expert consensus on the diagnosis and treatment of non-small cell lung cancer with MET alteration. Cancer biology Med. 2025, **22**(3)
30. C.M. Stellrecht, V. Gandhi, MET receptor tyrosine kinase as a therapeutic anticancer target. Cancer Lett. **280**(1), 1–14 (2009)
31. R. Yoshida, M. Saigi, T. Tani, B.F. Springer, H. Shibata, S. Kitajima, N.R. Mahadevan, M. Campisi, W. Kim, Y. Kobayashi et al., MET-Induced CD73 Restrains STING-Mediated Immunogenicity of EGFR-Mutant Lung Cancer. Cancer Res. **82**(21), 4079–4092 (2022)
32. S. Huang, Y. Long, Y. Gao, W. Lin, L. Wang, J. Jiang, X. Yuan, Y. Chen, P. Zhang, Q. Chu, Combined inhibition of MET and VEGF enhances therapeutic efficacy of EGFR TKIs in EGFR-mutant non-small cell lung cancer with concomitant aberrant MET activation. Experimental Hematol. Oncol. **13**(1), 97 (2024)
33. B. Lutterbach, Q. Zeng, L.J. Davis, H. Hatch, G. Hang, N.E. Kohl, J.B. Gibbs, B.S. Pan, Lung cancer cell lines harboring MET gene amplification are dependent on Met for growth and survival. Cancer Res. **67**(5), 2081–2088 (2007)
34. F. Cecchi, D.C. Rabe, D.P. Bottaro, Targeting the HGF/Met signalling pathway in cancer. Eur. J. cancer (Oxford England: 1990). **46**(7), 1260–1270 (2010)
35. P. Jamme, M. Fernandes, M.C. Copin, C. Descarpentries, F. Escande, A. Morabito, V. Grégoire, M. Jamme, S. Baldacci, D. Tulasne et al., Alterations in the PI3K Pathway Drive Resistance to MET Inhibitors in NSCLC Harboring MET Exon 14 Skipping Mutations. J. Thorac. oncology: official publication Int. Association Study Lung Cancer. **15**(5), 741–751 (2020)
36. J.K. Rotow, P. Gui, W. Wu, V.M. Raymond, R.B. Lanman, F.J. Kaye, N. Peled, F. Fece de la Cruz, B. Nadres, R.B. Corcoran et al., Co-occurring Alterations in the RAS-MAPK Pathway Limit Response to MET Inhibitor Treatment in MET Exon 14 Skipping Mutation-Positive Lung Cancer. Clin. cancer research: official J. Am. Association Cancer Res. **26**(2), 439–449 (2020)
37. G.L. Semenza, Targeting HIF-1 for cancer therapy. Nat. Rev. Cancer. **3**(10), 721–732 (2003)

38. G.N. Masoud, W. Li, HIF-1α pathway: role, regulation and intervention for cancer therapy. Acta Pharm. Sinica B **5**(5), 378–389 (2015)
39. D. Lin, J. Wu, Hypoxia inducible factor in hepatocellular carcinoma: A therapeutic target. World J. Gastroenterol. **21**(42), 12171–12178 (2015)
40. R. Riedel, J. Fassunke, H.L. Tumbrink, A.H. Scheel, C. Heydt, L. Hieggelke, M. Scheffler, A. Heimsoeth, L. Nogova, S. Michels et al., Resistance to MET inhibition in MET-dependent NSCLC and therapeutic activity after switching from type I to type II MET inhibitors. *European journal of cancer (Oxford, England*: 1990) 2023, 179:124–135
41. J.H. Lim, E.S. Lee, H.J. You, J.W. Lee, J.W. Park, Y.S. Chun, Ras-dependent induction of HIF-1alpha785 via the Raf/MEK/ERK pathway: a novel mechanism of Ras-mediated tumor promotion. Oncogene. **23**(58), 9427–9431 (2004)
42. E. Laughner, P. Taghavi, K. Chiles, P.C. Mahon, G.L. Semenza, HER2 (neu) signaling increases the rate of hypoxia-inducible factor 1alpha (HIF-1alpha) synthesis: novel mechanism for HIF-1-mediated vascular endothelial growth factor expression. Mol. Cell. Biol. **21**(12), 3995–4004 (2001)
43. H. Zhong, K. Chiles, D. Feldser, E. Laughner, C. Hanrahan, M.M. Georgescu, J.W. Simons, G.L. Semenza, Modulation of hypoxia-inducible factor 1alpha expression by the epidermal growth factor/phosphatidylinositol 3-kinase/PTEN/AKT/FRAP pathway in human prostate cancer cells: implications for tumor angiogenesis and therapeutics. Cancer Res. **60**(6), 1541–1545 (2000)
44. K. Koukoulas, A. Giakountis, A. Karagiota, M. Samiotaki, G. Panayotou, G. Simos, I. Mylonis, ERK signaling controls productive HIF-1 binding to chromatin and cancer cell adaptation to hypoxia through HIF-1α interaction with NPM1. Mol. Oncol. **15**(12), 3468–3489 (2021)
45. E.E. Wicks, G.L. Semenza, Hypoxia-inducible factors: cancer progression and clinical translation. J. Clin. Invest. 2022, **132**(11)
46. G. Peng, Y. Liu, Hypoxia-inducible factors in cancer stem cells and inflammation. Trends Pharmacol. Sci. **36**(6), 374–383 (2015)
47. M. Dean, T. Fojo, S. Bates, Tumour stem cells and drug resistance. Nat. Rev. Cancer. **5**(4), 275–284 (2005)
48. H.M. Zhou, J.G. Zhang, X. Zhang, Q. Li, Targeting cancer stem cells for reversing therapy resistance: mechanism, signaling, and prospective agents. Signal. Transduct. Target. therapy. **6**(1), 62 (2021)

Figures

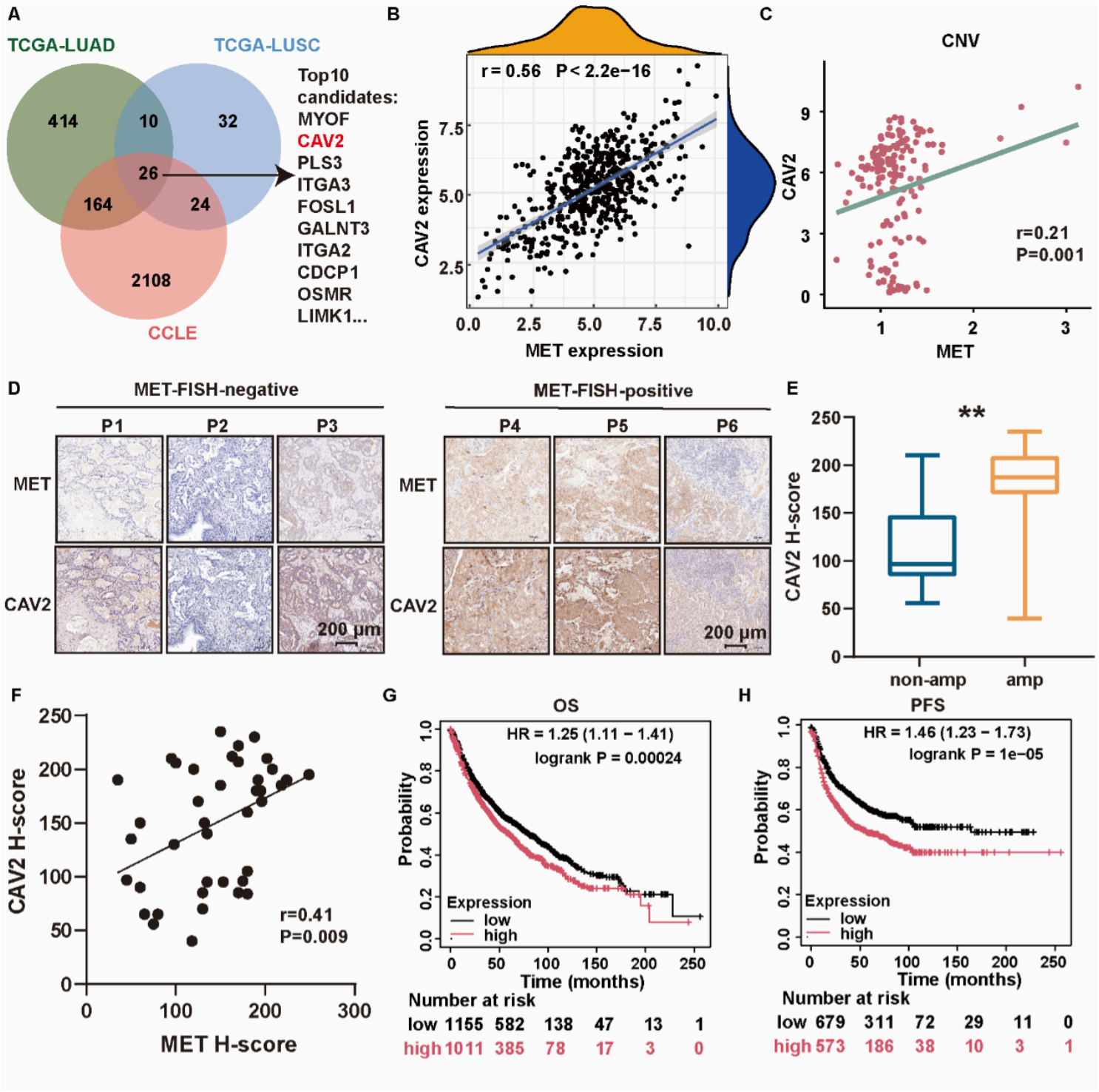

Figure 1

CAV2 expression is associated with MET status in NSCLC and with poorer survival in an independent public cohort.

(A) Integrated co-expression analysis of TCGA-LUAD, TCGA-LUSC, and CCLE datasets identified genes consistently associated with MET expression. (B) Correlation between MET and CAV2 expression. (C) Correlation between MET and CAV2 genomic copy-number alterations in NSCLC datasets. (D) Representative MET and CAV2 immunohistochemical staining in MET-FISH-negative and MET-FISH-

positive NSCLC specimens. Scale bars, 200 μm. (E) CAV2 H-scores in MET-FISH-negative and MET-FISH-positive specimens. (F) Correlation between MET and CAV2 H-scores. The fitted line and Spearman correlation statistics are shown. (G, H) Kaplan-Meier analyses of overall survival and progression-free survival according to CAV2 expression in an independent public NSCLC cohort. Data are presented as mean ± SD where applicable. Statistical significance was assessed using Student's t test, Spearman correlation analysis, or the log-rank test, as appropriate. *P < 0.05; **P < 0.01.

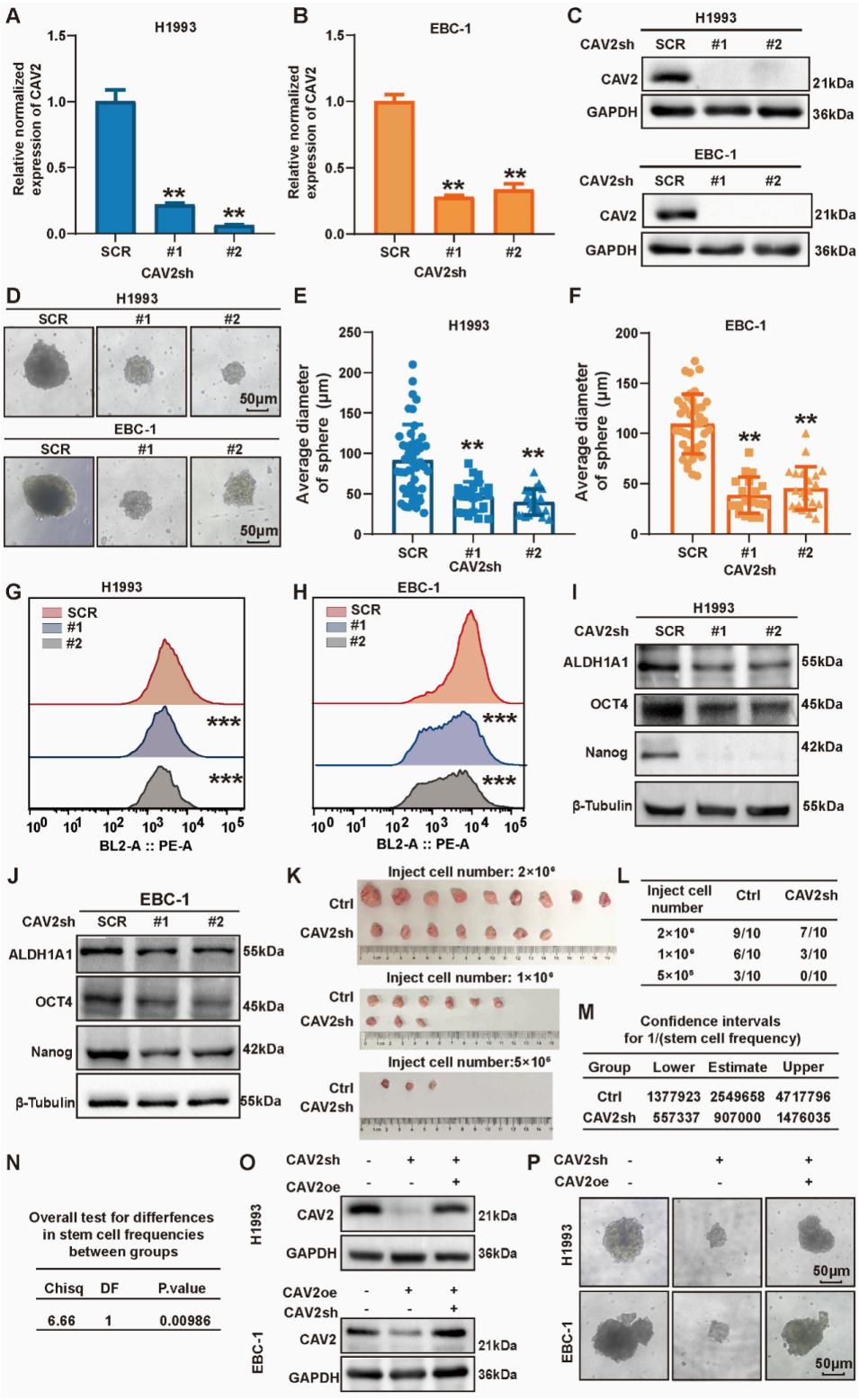

Figure 2

CAV2 sustains stemness-associated phenotypes in MET-amplified NSCLC cells.

(A-C) CAV2 knockdown in EBC-1 and H1993 cells was confirmed by qRT-PCR and western blotting. Full-length blots are shown in Supplementary Material 3, Fig. 1A. (D) Representative tumorspheres formed by control and CAV2-depleted cells. (E, F) Average tumorsphere diameter in H1993 and EBC-1 cells, respectively. (G, H) Representative flow cytometric histograms of CD44 expression in H1993 and EBC-1 cells. (I, J) Western blot analysis of ALDH1A1, OCT4, and NANOG after CAV2 depletion. Full-length blots are shown in Supplementary Material 3, Fig. 1B. (K) Representative tumors from the limiting dilution assay. (L) Tumor incidence at each cell dose. (M, N) ELDA estimates of tumor-initiating cell frequency. Control and CAV2-depleted H1993 cells were injected at 2×10^6, 1×10^6, or 5×10^5 cells per mouse in 100 μL of a 1:1 cell suspension and Matrigel mixture. Tumor formation was monitored for 30 days, with 10 mice per group at each dose. (O) Western blot confirmation of CAV2 re-expression. Full-length blots are shown in Supplementary Material 3, Fig. 1C. (P) Representative tumorspheres after CAV2 re-expression.

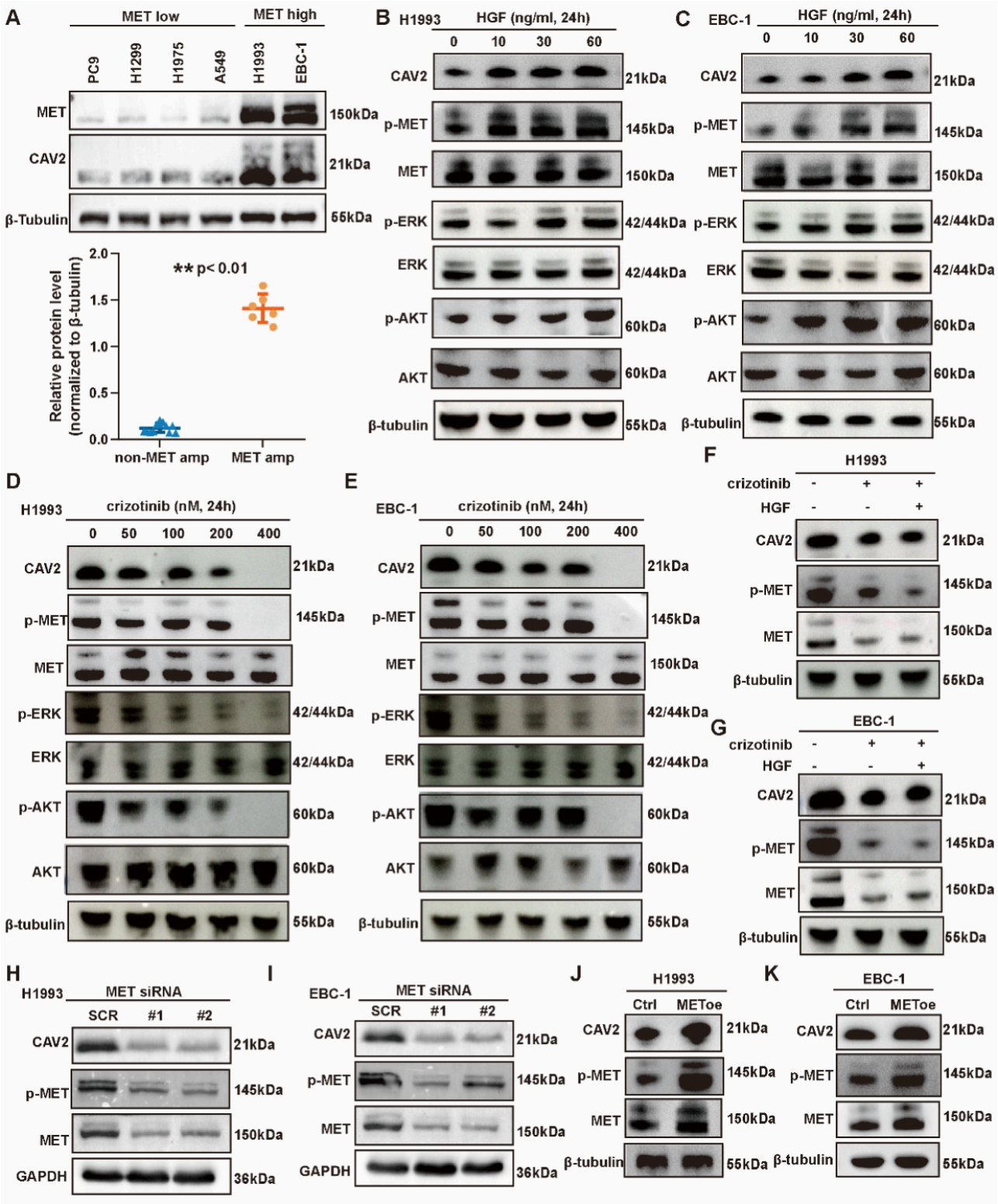

Figure 3

CAV2 expression is regulated by MET-associated signaling in NSCLC.

(A) Basal CAV2 protein expression in NSCLC cell lines with different MET activation states. Full-length blots are shown in Supplementary Material 3, Fig. 2A. (B, C) HGF stimulation increased CAV2 expression in H1993 and EBC-1 cells. Full-length blots are shown in Supplementary Material 3, Fig. 2B. (D-G)

Crizotinib treatment reduced CAV2 expression with or without HGF stimulation. Full-length blots are shown in Supplementary Material 3, Figs. 3 and 4A. (H, I) MET knockdown reduced CAV2 expression. Full-length blots are shown in Supplementary Material 3, Fig. 4B. (J, K) MET overexpression increased CAV2 expression. Full-length blots are shown in Supplementary Material 3, Fig. 4C, D. Data are presented as mean ± SD from at least three independent experiments. Statistical significance was assessed using Student's t test or one-way analysis of variance, as appropriate. *P < 0.05; **P < 0.01; ***P < 0.001.

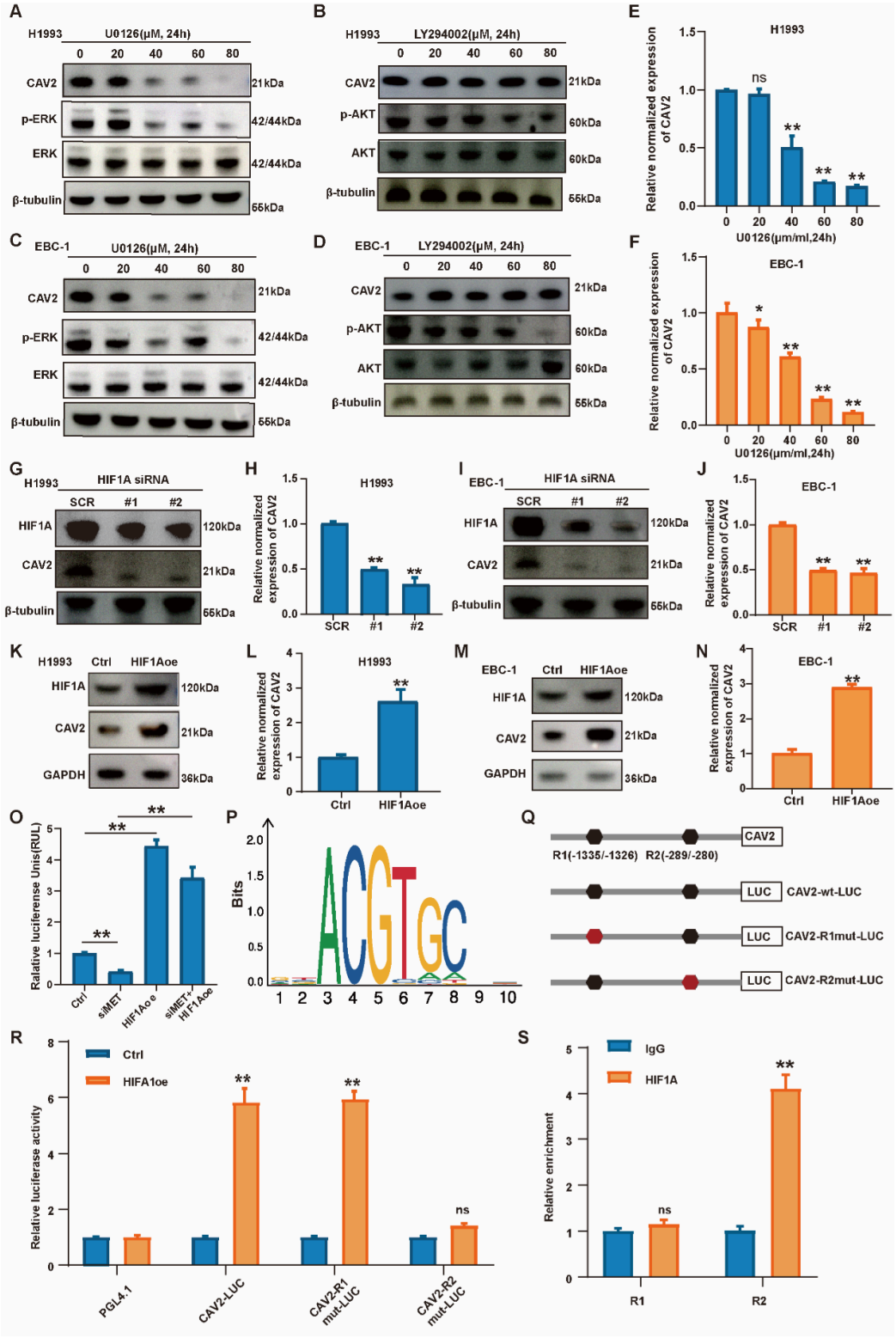

Figure 4

MET-associated signaling regulates CAV2 transcription through ERK and HIF1A.

(A-D) Western blot analysis of CAV2 and pathway activation in H1993 and EBC-1 cells treated with U0126 or LY294002. Full-length blots are shown in Supplementary Material 3, Fig. 5A, B. (E, F) CAV2 mRNA expression after treatment with increasing concentrations of U0126. (G-J) CAV2 expression after HIF1A knockdown. Full-length blots are shown in Supplementary Material 3, Fig. 5E. (K-N) CAV2 expression after HIF1A overexpression. Full-length blots are shown in Supplementary Material 3, Fig. 5F. (O) Effects of MET knockdown and HIF1A overexpression on CAV2 promoter activity. (P) Sequence logo of the predicted HIF-1α-binding motif. (Q) Wild-type and mutant CAV2 promoter reporter constructs. (R) Effects of HIF1A overexpression on wild-type and mutant promoter reporters. (S) ChIP-qPCR analysis of HIF-1α occupancy at the CAV2 promoter. Data are presented as mean ± SD from three independent experiments. Statistical significance was assessed using Student's t test or one-way analysis of variance with the indicated post hoc analysis. *P < 0.05; **P < 0.01; ***P < 0.001.

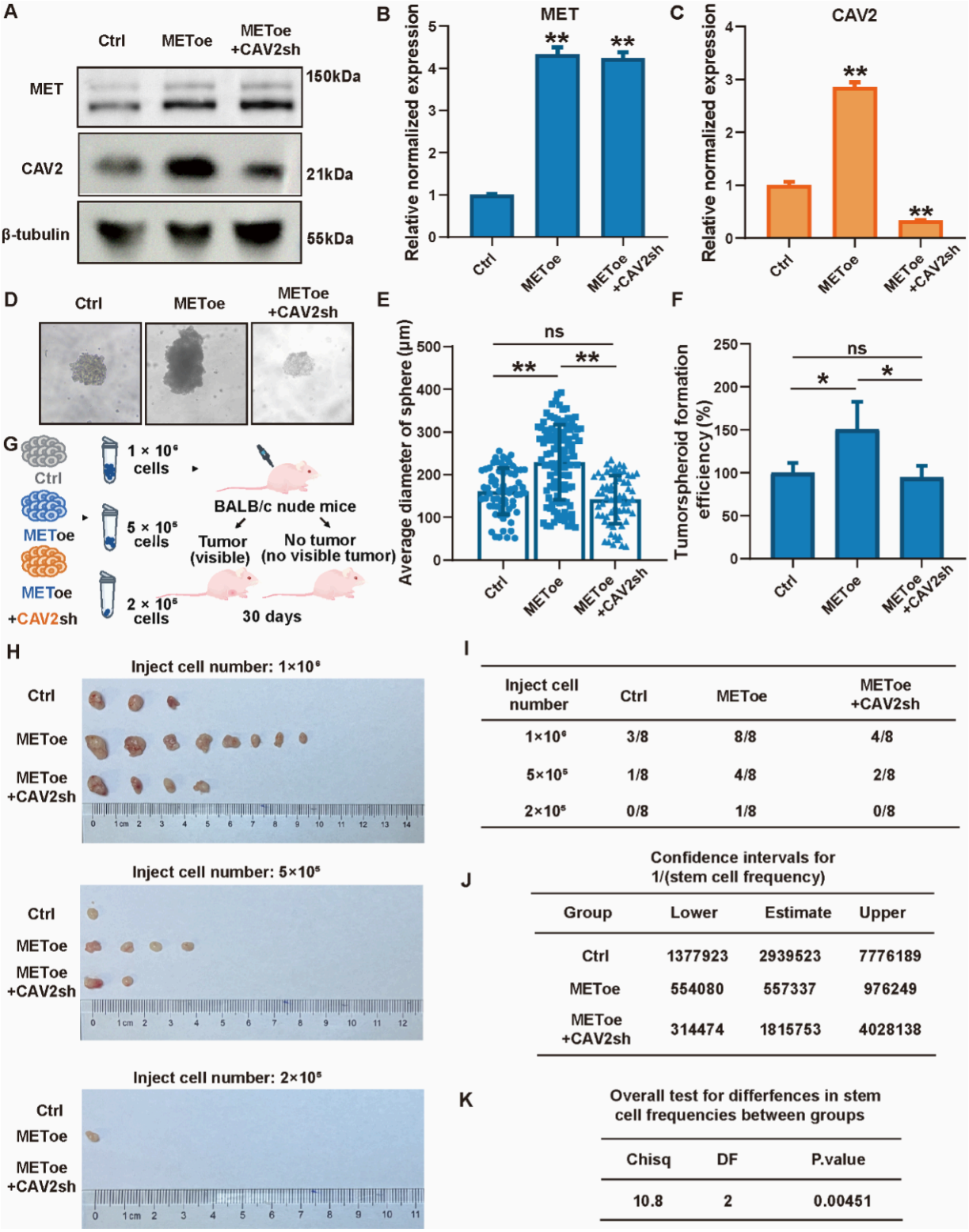

I

Inject cell number	Ctrl	METoe	METoe +CAV2sh
1×10⁵	3/8	8/8	4/8
5×10⁵	1/8	4/8	2/8
2×10⁵	0/8	1/8	0/8

J

Confidence intervals for 1/(stem cell frequency)

Group	Lower	Estimate	Upper
Ctrl	1377923	2939523	7776189
METoe	554080	557337	976249
METoe +CAV2sh	314474	1815753	4028138

K

Overall test for differfences in stem cell frequencies between groups

Chisq	DF	P.value
10.8	2	0.00451

Figure 5

CAV2 contributes to MET-induced stemness in NSCLC.

(A) Western blot confirmation of MET overexpression and CAV2 knockdown. Full-length blots are shown in Supplementary Material 3, Fig. 6A. (B, C) qRT-PCR analysis of MET and CAV2 expression. (D) Representative tumorspheres formed by control, MET-overexpressing, and MET-overexpressing/CAV2-

depleted cells. (E) Average tumorsphere diameter. (F) Tumorsphere formation efficiency. (G) Schematic of the limiting dilution xenograft assay. (H) Representative tumors at each cell dose. (I) Tumor incidence. (J, K) ELDA estimates of tumor-initiating cell frequency. Control, MET-overexpressing, and MET-overexpressing/CAV2-depleted cells were injected at 1 × 10^6, 5 × 10^5, or 2 × 10^5 cells per mouse in 100 µL of a 1:1 cell suspension and Matrigel mixture. Tumor formation was monitored for 30 days, with eight mice per group at each dose. Data are presented as mean ± SD from three independent experiments. Statistical significance was assessed using Student's t test or one-way analysis of variance with the indicated post hoc analysis. ELDA statistics were calculated using the ELDA software package. *P < 0.05; **P < 0.01; ***P < 0.001.

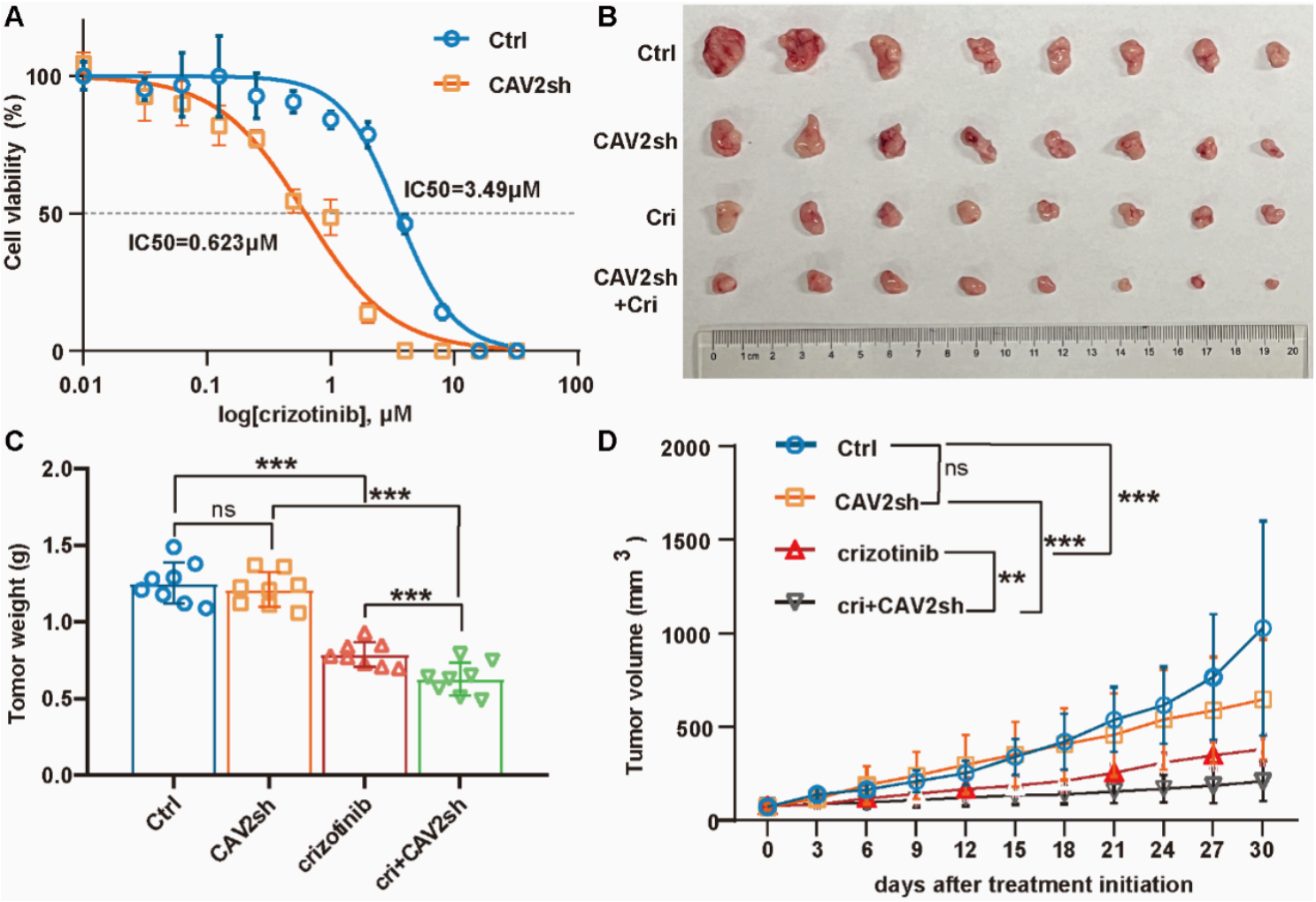

Figure 6

CAV2 depletion increases the response to crizotinib in MET-amplified NSCLC models.

(A) Crizotinib dose-response curves in control and CAV2-depleted H1993 cells. Cell viability was normalized to the untreated condition, and nonlinear regression was used to estimate IC_{50} values (control, 3.49 µM; CAV2sh, 0.623 µM). (B) Excised xenograft tumors after 30 days of vehicle or crizotinib treatment. Rows represent control plus vehicle, CAV2sh plus vehicle, control plus crizotinib, and CAV2sh plus crizotinib; n = 8 mice per group. (C) Endpoint tumor weights. Each point represents one mouse; bars

and error bars indicate mean ± SD. (D) Tumor volumes measured at treatment initiation and every 3 days for 30 days. Data are mean ± SD; n = 8 per group. Treatment began when individual tumors measured 50-100 mm^3, and tumor burden remained below the prespecified humane endpoint of 2,000 mm^3. Tumor weights were analyzed by one-way analysis of variance with Bonferroni's multiple-comparisons test. Tumor growth curves were analyzed by two-way repeated-measures analysis of variance followed by Bonferroni-adjusted comparisons. **P < 0.01; ***P < 0.001; ns, not significant.

Supplementary Files

This is a list of supplementary files associated with this preprint. Click to download.

- SupplementaryMaterial2.xls
- SupplementaryMaterial3.pdf
- SupplementaryMaterial1.docx
- ARRIVE2.0AuthorChecklist.pdf